Atmospheric
Chemistry
and Physics

Distribution, chemical, and molecular composition of high and low molecular weight humic-like substances in ambient aerosols

Xingjun Fan[1,2], Ao Cheng[1], Xufang Yu[1], Tao Cao[2,3], Dan Chen[1], Wenchao Ji[1], Yongbing Cai[1],
Fande Meng[1], Jianzhong Song[2], and Ping'an Peng[2]

[1]College of Resource and Environment, Anhui Science and Technology University,
Fengyang 233100, PR China
[2]State Key Laboratory of Organic Geochemistry, Guangzhou Institute of Geochemistry,
Chinese Academy of Sciences, Guangzhou 510640, PR China
[3]University of Chinese Academy of Sciences, Beijing 100049, PR China

Correspondence: Xingjun Fan (fanxj@ahstu.edu.cn) and Jianzhong Song (songjzh@gig.ac.cn)

Abstract. Humic-like substances (HULIS) encompass a continuum of molecular weight (MW) ranges, yet our understanding of how HULIS characteristics vary with MW is still limited and not well established. In this study, a combination of ultrafiltration and solid-phase extraction protocols was employed to fractionate the high MW (HMW; > 1 kDa) and low MW (LMW; < 1 kDa) HULIS fractions from ambient aerosols collected during summer and winter at a rural site. Subsequently, comprehensive characterization using total organic carbon, high-performance size exclusion chromatography (HPSEC), UV-visible (UV-vis) and fluorescence spectroscopy, Fourier transform infrared spectroscopy (FTIR), and negative electrospray ionization high-resolution mass spectrometry (ESI–HRMS) were conducted. The results revealed that HMW HULIS were dominated by larger-sized chromophores, substantially constituting a higher fraction of total organic carbon and UV absorption at 254 nm than LMW HULIS. While both HMW and LMW HULIS shared similar fluorophore types and functional groups, the former exhibited higher levels of humification and a greater presence of polar functional groups (e.g., −COOH; > C=O). HRMS analysis further unveiled that molecular formulas within HMW HULIS generally featured smaller sizes but higher degrees of unsaturation and aromaticity compared to those within LMW HULIS fractions. This observation suggests the possibility of small molecules assembling to form the HMW HULIS through intermolecular weak forces. Moreover, HMW HULIS contained a higher proportion of CHON but fewer CHO compounds than LMW HULIS. In both HMW and LMW HULIS, the unique molecular formulas were primarily characterized by lignin-like species, yet the former displayed a prevalence of N-enriched and highly aromatic species. Additionally, HMW HULIS contained more unique lipid-like compounds, while LMW HULIS exhibited a distinct presence of tannin-like compounds. These findings provide valuable insights into the distribution, optical properties, and molecular-level characteristics of HULIS in atmospheric aerosols, thereby advancing our understanding of their sources, composition, and environmental implications.

## 1	Introduction

Humic-like substances (HULIS) are complex and heterogeneous mixtures of water-soluble organic matter (WSOM) that are of great importance in the atmospheric environment. They usually share similar physicochemical properties (e.g., acidity, absorption, fluorescence, and functional groups) with naturally occurring humic substances (Zheng et al., 2013; Graber and Rudich, 2006) and are prevalent in fog, clouds, rainwater, and ambient aerosols (Birdwell and Valsaraj, 2010; Santos et al., 2012; Fan et al., 2016a). With substantial hygroscopic and surface-active properties, HULIS enhance the hygroscopic growth of particles, thereby contributing to the formation of cloud condensation nuclei and ice nuclei (Dinar et al., 2007; Chen et al., 2021a). Moreover, acting as an important component of brown carbon (BrC), HULIS effectively absorb near-ultraviolet and visible light, thus influencing the global radiative balance and atmospheric chemistry processes (Zhang et al., 2020; Bao et al., 2022). Furthermore, HULIS have the potential to catalyze the formation of reactive oxygen species, leading to potentially adverse health effects (Zhang et al., 2022b; Ma et al., 2019).

The chemical composition of atmospheric HULIS exhibits significant heterogeneity and typically comprises macromolecular compounds containing aromatic rings with highly conjugated structures, as well as long-chain hydrocarbon with polar groups (e.g., $-OH$, $-COOH$, and $-NO_2$) (Fan et al., 2013; Huo et al., 2021). To unravel the structural characteristics and properties of HULIS, a range of analytical techniques, including absorption and fluorescence spectroscopy, Fourier transform infrared spectroscopy (FTIR), and nuclear magnetic resonance spectroscopy (^{1}H NMR), have been utilized (Zou et al., 2020; Huo et al., 2021; Qin et al., 2022). These studies have provided insights into the overall structural characteristics of complex HULIS, including their abundances and chemical and optical characteristics (Zhang et al., 2022b; Mukherjee et al., 2020; Huo et al., 2021; Win et al., 2018; Zheng et al., 2013). In recent years, high-resolution mass spectrometry (HRMS) techniques, such as Fourier transform ion cyclotron resonance mass spectrometry (FT-ICR-MS) and Orbitrap HRMS, in combination with electrospray ionization (ESI), have emerged as powerful tools for elucidating the molecular-level characteristics of HULIS (Zou et al., 2023; Sun et al., 2021; Wang et al., 2019; Lin et al., 2012). By utilizing HRMS, researchers have gained deeper insights into the complexity and chemical heterogeneity of HULIS at the molecular level.

Operationally, HULIS are defined as the hydrophobic fraction of water-soluble organic matter (WSOM) typically extracted through the solid-phase extraction (SPE) protocol (Fan et al., 2012; Zou et al., 2020). Thus, the abundance and characteristics of HULIS are contingent upon the chemical composition of WSOM. Previous studies have shown that aerosol WSOM, often seen as water-soluble brown carbon (BrC), is comprised of a continuum of molecular weight

(MW) species, as revealed by high-performance size exclusion chromatography (HPSEC) analysis (Di Lorenzo et al., 2017; Wong et al., 2019; Fan et al., 2023). These studies have highlighted that BrC typically consists of both high MW (HMW) and low MW (LMW) chromophores in various aerosols. For example, BrC emitted from fresh biomass burning (BB) is dominated by low MW chromophores (Di Lorenzo et al., 2017; Wong et al., 2019). However, BrC derived from aged BB aerosols and ambient aerosols tends to possess more HMW chromophores that are highly chemically resistant (Di Lorenzo et al., 2017; Wong et al., 2019; Fan et al., 2023). Further characterizations of different MW BrC can be conducted using an ultrafiltration (UF) protocol (Fan et al., 2021). This approach enabled researchers to obtain the distributions of the content, chromophores, and fluorophores within various MW BrC fractions. Despite these advancements, the chemical structures and molecular composition of different MW HULIS fractions remain poorly understood. Consequently, a combination of UF and SPE protocols for the fractionation and the characterization of MW-separated HULIS is crucial, as it not only provides insights into MW distributions but also illuminates the chemical heterogeneities of aerosol HULIS.

In this study, a combination of the UF–SPE isolation protocol was developed to fractionate and characterize the MW HULIS fractions. Two distinct sets of ambient $PM_{2.5}$ samples collected during summer and winter periods were utilized to facilitate a comparative analysis of MW HULIS. Initially, the WSOM were fractionated into high MW (HMW, $> 1\,kDa$) and low MW (LMW, $< 1\,kDa$) species using the UF protocol. Subsequently, the resulting MW WSOM fractions underwent SPE to obtain different MW HULIS fractions. The obtained HMW and LMW HULIS fractions were comprehensively characterized using advanced analytical techniques, including total organic carbon analysis, UV visible (UV-vis) and fluorescence spectroscopy, HPSEC, and HRMS to unveil their abundances, absorption, and fluorescence properties, and molecular characteristics. The findings of this study hold great significance in advancing our understanding of the definition and molecular profiles of HULIS, as well as facilitating further investigations into their potential impacts on the atmospheric environment.

## 2	Materials and methods

### 2.1	Atmospheric fine particles sampling

Atmospheric $PM_{2.5}$ were sampled on the rooftop of a building within the campus of Anhui Science and Technology University ($32.21°$ N, $118.72°$ E), around $20\,m$ above ground level. Detailed information regarding the sampling site can be found in our previous studies (Fan et al., 2021; Cao et al., 2023). The $PM_{2.5}$ samples were collected using a high-volume $PM_{2.5}$ sampler (JCH-1000, Juchuang Group Co., Ltd, Qingdao, China) onto prebaked quartz fiber filters

(20 × 25 cm, Whatman). Sampling took place from 25 July to 12 August 2021, during summer, and from 19 December 2021 to 6 January 2022, during winter. Blank filters were also collected as control samples. All aerosol PM$_{2.5}$ filter samples were stored at −20 °C in a freezer prior to analysis. The atmospheric pollutant data (NO$_2$, SO$_2$ and O$_3$) near the sampling site during sampling period were obtained from the website (https://www.aqistudy.cn, last access: 8 March 2023) and are summarized in Table S1 in the Supplement. Additionally, the fire spots were investigated using data from the website (https://firms.modaps.eosdis.nasa.gov/map/, last access: 8 March 2023) and are visualized in Fig. S1 in the Supplement.

2.2 Application of UF–SPE for isolating MW HULIS fractions

Punches of summer and winter aerosol PM$_{2.5}$ filter samples were taken and combined for the extraction of water-soluble organic matter (WSOM), respectively. The filters were immersed in 300 mL of ultrapure water and subjected to ultrasonication for 30 min. The resulting suspensions were then filtered through a 0.22 µm membrane (Φ 47 mm, Jinteng Experimental Equipment Co., Ltd., Tianjin, China) to obtain bulk WSOM samples. These bulk filtrates were further subjected to UF and SPE in tandem to obtain different MW HULIS fractions. Please refer to Fig. S2 for a schematic representation of the fractionation steps.

Before UF, the bulk WSOM were diluted to DOC concentration below 30 mg L^{-1} to minimize the concentration effects and prevent the accumulation of organic matter at the membrane surface during UF. The detailed UF procedure followed the profile described in our previous study (Fan et al., 2021). Briefly, each bulk WSOM solution was passed through a pre-cleaned 1 kDa cutoff membrane in a stirred UF cell (Amicon 8200, Millipore, USA), with a pressure at 0.2 MPa applied by ultrapure N$_2$. The concentration factor was ∼ 10. The resulting retentate was considered HMW (> 1 kDa) WSOM, while the permeate solutions represented the LMW (< 1 kDa) WSOM. Finally, each MW fraction was diluted to the initial volume for further treatment and analysis. Mass balances of WSOM during one-step UF process generally ranged from 92 % to 99 %, as determined by total organic carbon (TOC) and UV absorption at 254 nm (UV$_{254}$), indicating good performance of UF without substantial loss or organic contamination.

Subsequently, SPE was applied to isolate the so-called HULIS fractions from the bulk and each MW fraction of WSOM, following the protocol proposed in our previous studies (Zou et al., 2020; Fan et al., 2013). Briefly, the acidified aqueous samples were passed through preactivated HLB (hydrophilic/lipophilic balanced polymer) columns (Waters Oasis, 500 mg/6 mL, USA). The fractions retained on the resins (referred to as HULIS) were eluted with pure methanol and dried using a gentle stream of pure

N$_2$. Finally, the bulk, HMW HULIS fractions, and LMW HULIS fractions were obtained. A blank filter control was performed using the same procedure described above, and the analysis signals of samples were corrected by blank control.

2.3 HPSEC analysis

The apparent MW distributions of MW HULIS fractions were analyzed using a high-performance liquid chromatography (HPLC) system (LC-20AT, Shimadzu, Japan) equipped with a refractive index detector (RID-10A, Shimadzu) and a diode array detector (SPD-M20A, Shimadzu, Japan). The wavelength of the diode array detector was set at 254 nm. Separation was performed using an aqueous gel filtration column (PolySep-GFC-P 3000, Phenomenex) preceded by a guard column (PolySep-GFC-P, Phenomenex). The mobile phase consisted of a mixture of water and methanol (90 : 10 v/v) containing 25 mM ammonium acetate (Di Lorenzo et al., 2017; Wong et al., 2019). The sample injection volume was 100 µL, and the flow rate was maintained at 1 mL min^{-1}. The HPSEC calibration was performed using a series of polyethylene glycol (PEG) standards (Kawasaki et al., 2011; Zhang et al., 2022). The chromatographic peak areas were integrated to represent the abundances of corresponding MW species. It should be noted that the MW values estimated here are nominal rather than absolute due to the lack of appropriate standards for column calibration (Fan et al., 2023; Wong et al., 2017).

The weight-averaged MW (Mw), number-averaged MW (Mn) and polydispersivity (ρ), were determined using the following equations (Song et al., 2010):

$$\text{Mw} = \frac{\sum_{i=1}^{n}(h_i \text{MW}_i)}{\sum_{i=1}^{n} h_i} \tag{1}$$

$$\text{Mn} = \frac{\sum_{i=1}^{n} h_i}{\sum_{i=1}^{n}(h_i/\text{MW}_i)} \tag{2}$$

$$\rho = \frac{\text{Mw}}{\text{Mn}}, \tag{3}$$

where h_i and MW$_i$ are the absorption intensity of the chromatogram and the MW of molecules corresponding to the ith retention time, respectively.

2.4 Measurements of WSOC content and optical properties

The concentration of water-soluble organic carbon (WSOC) in HMW and LMW HULIS was measured using a Shimadzu TOC analyzer (TOC-V CPH, Japan), following the non-purgeable organic carbon protocol.

The UV-vis spectra were recorded using a UV-vis spectrophotometer (UV-2600, Shimadzu, Japan) over a wavelength range of 200–700 nm with 1 nm increments. Excitation emission matrix (EEM) spectra were determined using a fluorescence spectrophotometer (F-4600, Hitachi, Japan). The scanning ranges for excitation (Ex) and emission (Em) wavelengths were 200–400 and 290–520 nm, respectively, with a scanning speed of 12 000 nm min⁻¹.

To characterize the chemical and optical properties of MW HULIS fractions, several commonly used spectra parameters were calculated, including the specific UV absorbance at 254 nm ($SUVA_{254}$), the UV absorbance ratio between 250 and 365 nm (E_2/E_3), spectra slope ratios (S_R), the absorption Ångström exponent (AAE), and mass absorption efficiency (MAE_{365}), fluorescence index (FI), biological index (BIX), and humification degree (HIX) (Li et al., 2022; Fan et al., 2021; Wu et al., 2021). Further details can be found in Text S1 of the Supplement.

2.5 HRMS analysis and data processing

The MW HULIS fractions were analyzed using a Q Exactive mass spectrometer (Thermo Scientific, Germany) equipped with a heated electrospray ionization (ESI) source. The system operated in negative ESI mode with a resolution of 140 000 at $m/z = 200$. The detection mass range was set from m/z 60 to 900. To ensure accurate mass measurements, mass calibration was carried out using a commercial standard mixture of ESI-L Low Concentration Tuning Mix (G1969-85000, Agilent, USA). It is important to note that the negative ESI source is more sensitive to detecting polar acid compounds, and the reported specific chemical composition here represents a fraction that is ionized in a biased manner in the negative ESI source and not the entire HULIS composition (He et al., 2023; Song et al., 2022).

The acquired mass spectra were processed using Xcalibur software (V2.2, Thermo Scientific). The mathematically possible formulas for all ions were calculated with a signal-to-noise ratio (S/N) ≥ 5, using a mass tolerance of 5 ppm. The assigned molecular formulas followed specific constraints, with limitations on the following elements: C ≤ 50, H ≤ 100, O ≤ 20, N ≤ 3, and S ≤ 2. Additionally, the elemental ratios of H/C, O/C, N/C, and S/C were constrained to the ranges of 0.3–3.0, 0–3.0, 0–0.5, and 0–2.0, respectively. The double-bond equivalents (DBEs) and modified aromaticity index (AI_{mod}) values of the assigned formula ($C_cH_hO_oN_nS_s$) were calculated using Eqs. (4)–(5) (Song et al., 2022; He et al., 2023):

$$DBE = 1 + \frac{1}{2}(2c - h + n) \tag{4}$$

$$AI_{mod} = \frac{1 + c - 0.5o - 0.5n - 0.5h}{c - 0.5o - n}. \tag{5}$$

The intensity-weighted molecular parameters (X_W) of MW, H/C, O/C, DBEs, and AI values were calculated according to Eq. (6) (He et al., 2023; Zou et al., 2023; Zhang et al., 2021):

$$X_W = \frac{\sum(I_i \cdot X_i)}{\sum I_i}, \tag{6}$$

where X represents the aforementioned parameters, and I_i values denote the intensity for each assigned formula i.

3 Results and discussion

3.1 Size and distribution of MW HULIS fractions

3.1.1 Molecular size of HMW and LMW HULIS

Due to the potential differences in molecular densities between the calibration standards (PEG) and BB WSOC, the reported molecular weight of HULIS calculated by HPSEC herein is only estimate. Figure 1 shows the HPSEC chromatograms of MW HULIS. Both HMW and LMW HULIS exhibit MW continuum distributions ranging from 100 to 20 000 Da, which is consistent with the reported distributions of BrC in BB-derived and various ambient aerosol in previous studies (Di Lorenzo et al., 2017; Wong et al., 2017; Fan et al., 2023). However, the chromatographic patterns for HMW HULIS clearly differ from those observed for LMW HULIS in both aerosol samples. As seen in Fig. 1, HMW HULIS display an additional and stronger absorption peak at around 4000 Da (peak iii), along with a more pronounced peak at 2200 Da (peak ii) and a similar magnitude peak at 570 Da (peak i) compared to LMW HULIS. This suggests that HMW HULIS contain the majority of larger molecular size chromophores within the bulk WSOM. In addition, the magnitude peak at 570 Da (peak i) in HMW HULIS may indicate the incorporation of small molecules through weak interactions, based on π–π and/or van der Waals forces between the HULIS components (Fan et al., 2021; Piccolo, 2002).

Moreover, the molecular size of MW HULIS can be further reflected by the differences in Mw and Mn. As listed in Table 1, the average Mw and Mn values of HMW HULIS are 2233–2315 and 654–707 Da, respectively, which are much larger than that of LMW HULIS (989–1071 and 293–394 Da, respectively). Note that these values are estimates rather than absolute, given the absence of the appropriate aerosol HULIS standards (Fan et al., 2023; Wong et al., 2017). Moreover, these differences indicate that the sources and formation processes of HMW HULIS may differ from LMW HULIS. Many previous studies have demonstrated that fresh BB HULIS generally consist of small molecular-sized chromophores (Di Lorenzo et al., 2018, 2017; Wong et al., 2017, 2019). However, a notable enhancement in the formation of large molecular-sized chromophores has been found when they undergo intricate atmospheric processes (Di Lorenzo et al., 2018, 2017; Wong et al., 2017, 2019). Based on these limited studies, it is suggested that HMW HULIS, characterized by higher proportions of large-sized chromophores and
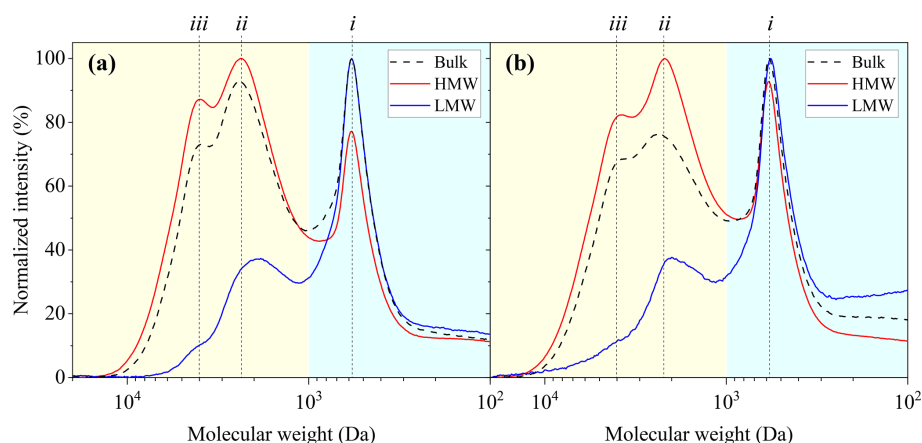
Figure 1. Average HPSEC chromatograms of bulk, HMW HULIS fractions, and LMW HULIS fractions in (a) summer and (b) winter aerosol, respectively. The yellow and cyan shadows represent MW size regions of > 1 and < 1 kDa, respectively.

the resulting larger apparent molecular size, might be associated with the products from atmospheric aging process rather than being emitted directly by primary sources.

3.1.2 Relative abundances of HMW and LMW HULIS

The contribution of MW HULIS fractions to their corresponding MW WSOM fractions, quantified in terms of TOC and UV absorption at 254 nm for both summer and winter aerosols, is summarized in Table 1. In general, the ratios of HULIS / WSOM of HMW fractions (in terms of TOC and UV254) (65 %–68 %) were higher than the ratios (41 %–61 %) observed for LMW fractions. This finding suggests that the higher presence of hydrophobic and conjugated aromatic structures in HMW WSOM but more hydrophilic organic carbon (OC) and non-aromatic species (e.g., aliphatic dicarboxylic acid) in the LMW WSOM (Fan et al., 2012; Zou et al., 2020).

Figure 2 illustrates the distribution of distinct MW fractions within reconstructed WSOM, where "non-HULIS" refers to the content differences between the MW WSOM and its HULIS fractions. The HMW HULIS fraction contributed 39 %–41 % of TOC and 40 %–47 % of UV254 to the bulk WSOM. In contrast, the LMW HULIS fraction only makes up a smaller proportion, accounting for 16 %–20 % of TOC and 17 %–21 % of UV254 within the bulk WSOM. Specifically, the ratios between HMW HULIS and LMW HULIS (H/L) ranged from 1.88 to 2.75 for both summer and winter aerosols in terms of either TOC or UV254. These findings emphasize that HMW HULIS significantly dominate the bulk aerosol HULIS fractions. Notably, the H/L ratio for winter aerosols was higher than that for summer aerosols, suggesting that larger-sized HULIS contributed more to the bulk HULIS fractions in winter aerosols.

The non-HULIS fractions are also important constituents within aerosol WSOM but exhibit some differences between HMW and LMW fractions. The contributions of HMW non-
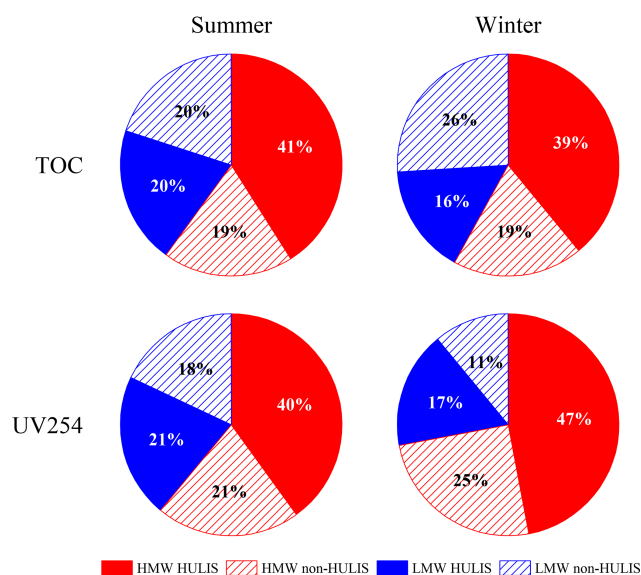
Figure 2. Relative proportions of different MW fractions in summer and winter aerosols determined by TOC and UV254.

HULIS to bulk WSOM were ∼ 19 %, as determined by TOC and 21 %–25 % measured by UV254. In case of LMW non-HULIS, the contributions were higher in terms of TOC (20 %–26 %) but lower in terms of UV254 (11 %–18 %). These results indicate that the LMW WSOM contains a larger proportion of hydrophilic organic species with weaker light absorption.

3.2 Optical characteristics of MW HULIS fractions

3.2.1 Light absorption characteristics

The absorption spectra of MW HULIS fractions in ambient aerosols are shown in Fig. S3. These spectra exhibit a featureless shape with a general decrease in absorbance as

Table 1. The summary of typical quantity and quality parameters of each MW HULIS fraction from BB and ambient aerosols.

		Summer			Winter		
		Bulk	HMW	LMW	Bulk	HMW	LMW
HPSEC-derived parameters	M_w	1975 ± 13	2315 ± 38	1071 ± 24	1918 ± 56	2233 ± 42	989 ± 67
	M_n	591 ± 53	707 ± 48	394 ± 13	525 ± 57	654 ± 17	293 ± 32
	ρ	3.4 ± 0.3	3.3 ± 0.2	2.7 ± 0.2	3.7 ± 0.3	3.4 ± 0.2	3.4 ± 0.2
HULIS/WSOM (%)*	TOC	65 ± 1	68 ± 1	51 ± 2	63 ± 2	67 ± 2	41 ± 1
	UV_{254}	66 ± 5	65 ± 2	55 ± 4	67 ± 1	65 ± 1	61 ± 2
Optical parameters	E_2/E_3	12.02 ± 0.54	11.72 ± 0.31	14.98 ± 0.98	6.30 ± 0.24	6.54 ± 0.16	7.24 ± 0.43
	MAE_{365}	0.21 ± 0.02	0.23 ± 0.01	0.20 ± 0.01	1.04 ± 0.02	1.06 ± 0.01	0.88 ± 0.00
	AAE	7.11 ± 0.32	7.59 ± 0.00	8.25 ± 0.23	6.66 ± 0.06	6.25 ± 0.06	7.28 ± 0.03
	FI	2.00 ± 0.04	1.99 ± 0.03	2.04 ± 0.05	2.06 ± 0.01	1.97 ± 0.03	2.25 ± 0.02
	BIX	0.95 ± 0.01	0.86 ± 0.07	1.02 ± 0.01	0.96 ± 0.01	0.81 ± 0.01	1.07 ± 0.02
	HIX	2.42 ± 0.06	2.43 ± 0.04	2.40 ± 0.05	3.13 ± 0.25	5.64 ± 0.34	1.94 ± 0.16

* The ratios of the contents of SPE-isolated HULIS fractions to that of corresponding WSOM fractions are determined by TOC and/or absorbance at 254 nm (UV_{254}).

the wavelength increases, which is a typical characteristic of HULIS found in rainwater, biomass burning (BB), and ambient aerosols (Santos et al., 2009; Huo et al., 2021; Zhang et al., 2022b). The E_2/E_3 ratio, commonly used as an indicator of the chemical characteristics of organic species, is inversely correlated with higher aromaticity and larger molecular weight (Li et al., 2022; Fan et al., 2021; Sun et al., 2021). As listed in Table 1, the E_2/E_3 of HMW HULIS fractions generally were lower than that of LMW HULIS in both ambient aerosols. This is consistent with the expectation that larger-sized HULIS generally possess more polyconjugated and polymeric structures (Fan et al., 2021; Zhang et al., 2022), leading to greater aromaticity and larger molecular size.

MAE$_{365}$ and AAE are commonly used to characterize the light absorption capacity and the spectral dependence of light absorption by aerosol chromophores, respectively (Bao et al., 2022; Fan et al., 2016b; Yuan et al., 2021; Kumar et al., 2017; Zou et al., 2020). As listed in Table 1, the average MAE$_{365}$ values of HMW HULIS are 0.23 and $1.06 \, \mathrm{m^2 \, g^{-1}}$ in summer and winter aerosol, respectively. These values are higher than the corresponding values of 0.20 and $0.88 \, \mathrm{m^2 \, g^{-1}}$, respectively, for LMW HULIS. In addition, HMW HULIS presented lower AAE values, with 7.59 and 6.25 in summer and winter aerosol, respectively, than the corresponding values of 8.25 and 7.28, respectively, for LMW HULIS (Table 1). These findings are consistent with the observation in our previous study that larger WSOM generally have higher MAE$_{365}$ but smaller AAE values than smaller WSOM (Fan et al., 2021). Generally, the results suggest that HMW HULIS exhibit stronger light-absorbing ability but with light absorption showing a weaker wavelength dependence. It is worth noting that combustion sources, such as BB and coal combustion, usually emit primary HULIS with high MAE$_{365}$ values due to the enrichment of polyaromatic and unsaturated

species (Cao et al., 2021; Fan et al., 2018; Huo et al., 2021; Zhang et al., 2021) but with small molecular weight distributions (Di Lorenzo et al., 2018, 2017; Wong et al., 2017). Furthermore, subsequent pronounced photooxidation and photobleaching processes can lead to an enrichment and/or a formation of large-sized chromophores (Di Lorenzo et al., 2018, 2017; Wong et al., 2017), concurrently resulting in a reduction in their absorption capacity and an enhancement of their spectra dependence on wavelength (Zhang et al., 2022a; Wu et al., 2018, 2020; Chen et al., 2021b; Fan et al., 2019). From this perspective, the secondary organic aerosol (SOA) formation might induce the generation of HMW HULIS with lower light absorption capacity and weaker light absorption wavelength dependence. In contrast, LMW HULIS is more likely to represent small-sized primary HULIS and/or by-products resulting from the degradation and oxidation of primary large-sized HULIS. Considering the complex sources of ambient HULIS, future studies should explore the MW-dependent light absorption characteristics of HULIS from different sources.

3.2.2 Fluorescence characteristics

The EEM contours of MW HULIS fractions from both summer and winter aerosols are presented in Fig. S4. These HULIS fractions from both seasons exhibit similar EEM spectra features, with a predominance of humic-like fluorophores (Ex/Em = 210–235/395–410 nm). This observation suggests that humic-like fluorophores are fundamental constituents of both HMW and LMW HULIS, which are consistent with previous findings for aerosol MW WSOM (Fan et al., 2021) and bulk HULIS in BB-derived and ambient aerosols (Qin et al., 2018; Fan et al., 2020). The findings imply an assembly of small and heterogeneous molecules to form bulk HULIS through weak intramolecular forces (i.e.,

$\pi-\pi$, van der Waals, hydrophobic, or hydrogen bonds) (Piccolo, 2002; Fan et al., 2021) and/or charge–transfer interactions (Phillips et al., 2017; Qin et al., 2022). In this study, the fluorescence regional integration (FRI) method was applied to characterize the fluorescent composition of MW HULIS. Using FRI, EEM spectra were divided into five fluorescence regions (labeled I to V) (Fig. S4), which were successively assigned to simple aromatic proteins (I and II) and fulvic-acid-like (III), soluble microbial byproduct-like (IV), and humic-acid-like (V) substances, respectively, as established in previous studies (Qin et al., 2018; Chen et al., 2003; Wang et al., 2021b). As shown in Fig. S5, the large-sized aromatic proteins (II) and fulvic-acid-like substances (III) dominated the fluorophores within MW HULIS in both summer and winter aerosols, comprising approximately 62 %–64 % of the total fluorescence intensity. This finding is consistent with previous reports on bulk HULIS in summer and winter aerosols from industrial and urban cities (Qin et al., 2018; Wang et al., 2021b). In comparison, the HMW HULIS in both summer and winter aerosols generally exhibited a higher proportion of humic-acid-like substances (V), while having a lower abundance of small-sized aromatic proteins (I) compared to LMW HULIS. These differences are particularly pronounced in winter aerosols, with the humic-acid-like substances accounting for 23 % in HMW HULIS compared to 13 % in LMW HULIS, and small-sized aromatic proteins (I) comprising 9 % in HMW HULIS compared to 17 % in LMW HULIS (Fig. S5). Furthermore, the higher HIX values of HMW HULIS (5.64) in comparison to LMW HULIS (1.94) further support these differences (Table 1). The pronounced BB emissions and potential NO_2-related oxidation of organic aerosol (OA), as evidenced by the presence of more hotspots (Fig. S1) and higher concentration of NO_2 (Table S1), are likely driving these marked distinctions between HMW and LMW HULIS in winter aerosols. In general, these findings imply that the HMW HULIS have a stronger level of humification and oxidation, while the LMW HULIS appear to be of a simpler nature and are more likely associated with fresh emissions (e.g., BB).

3.3 Molecular-level insights into MW HULIS

3.3.1 Seasonal variations in the molecular composition of MW HULIS

The molecular-level characteristics of MW HULIS were examined using negative ESI–HRMS analysis. It is worth noting that the ESI–HRMS could reveal the molecular composition of a subset of organic molecules that are biased towards ionization in the negative ESI source, particularly for acid compounds such as carboxylic and sulfonic acids, and may not represent the entire HULIS composition (He et al., 2023; Lin et al., 2012). Additionally, HRMS techniques are often known to be biased towards low masses below 600 Da (Lin et al., 2012; Wang et al., 2019), suggesting that the molecu-

lar sizes calculated by HRMS are likely underestimated. Figure 3 displays the reconstructed mass spectra of all HULIS fraction in both summer and winter aerosols. Hundreds of peaks can be observed in the spectra ranging from m/z 100 to 450 for all samples, with most ions being abundant within the m/z 150–350 range. These spectrum characteristics are similar to the low m/z range previously reported for HULIS in ambient aerosols and BB emissions (He et al., 2023; Sun et al., 2021; Zou et al., 2023; Wang et al., 2019; Song et al., 2022; Zhang et al., 2021). The similarity in low m/z range among HMW and LMW HULIS and other bulk HULIS may indicate their shared fundamental molecules, further suggesting the potential disassembly of larger molecules.

As listed in Table 2, the number of assigned formulas within MW HULIS in summer aerosols was 655–672, which was higher than the range of 470–506 observed in winter aerosols. This suggests that the MW HULIS in summer aerosols exhibited greater diversity than those in winter aerosols, mainly due to the stronger SOA formation that enhanced the heterogeneity of HULIS fractions in the summer. Moreover, SOA-derived HULIS generally contain more polar molecules (e.g., $-OH$ and $-COOH$) (Di Lorenzo et al., 2017; Fan et al.,2020; Huo et al., 2021), making them more susceptible to deprotonation and leading to the generation of a greater number formulas under negative ESI conditions. The identified formulas were then classified into four groups (i.e., CHO, CHON, CHOS, and CHONS) according to their elemental composition. As depicted in pie charts in Fig. 3, summer HULIS are predominantly composed of CHO (54 %–71 %), while winter HULIS feature a high concentration of both CHON (30 %–58 %) and CHO (21 %–38 %). The notably higher content of CHO in summer HULIS are likely due to a wide distribution of biogenic volatile organic carbon (BVOC)-derived SOAs during the summer season (Sun et al., 2023; Li et al., 2022). CHON content in winter HULIS is generally higher than in summer ones, potentially due to more significant contributions from direct BB, as well as secondary nitrogen-related chemical processes during the winter season (He et al., 2023; Song et al., 2022; Zou et al., 2023; Zhang et al., 2021). This finding is supported by the greater number of fire spots (Fig. S1) and higher concentrations of NO_2 (Table S1) during winter. The higher proportions of CHON compounds in aerosol HULIS typically lead to enhanced light absorption capabilities (He et al., 2023; Song et al., 2022; Zeng et al., 2021). This provides a potential explanation for the higher MAE_{365} values observed in winter HULIS compared to summer HULIS. Additionally, CHOS is more abundant in winter HULIS (17 %–25 %) than in summer aerosols (13 %–18 %). Previous studies have demonstrated that both coal combustion and the oxidation initiated by SO_2 can lead to the generation of larger numbers of S-containing compounds (Song et al., 2022; Zou et al., 2023; Song et al., 2018). This finding suggested that the increased levels of coal combustion and SO_2-related SOAs, as evidenced by higher concentration of SO_2 (Table S1), are
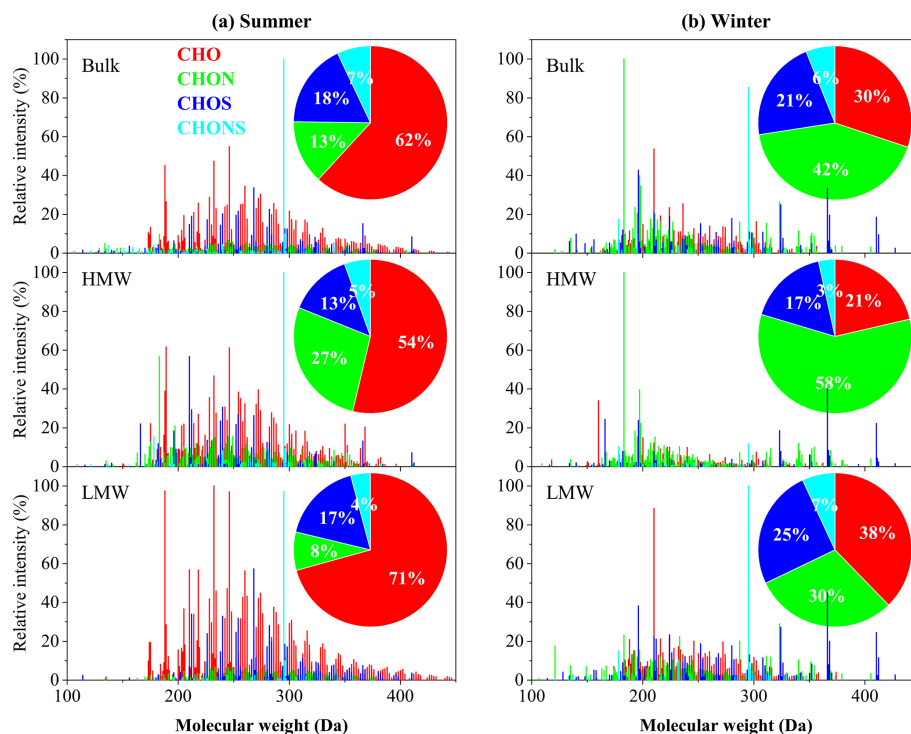
Figure 3. Mass spectra of bulk and MW HULIS in **(a)** summer and **(b)** winter aerosols. The pie charts represent the intensity distributions of four compound categories (CHO, CHON, CHOS, and CHONS).

significant contributors to the presence of BrC in winter compared to in summer.

Table 2 summarizes the intensity-weighted molecular parameters for MW HULIS in both summer and winter aerosols. Evidently, the MW_w of summer HULIS are 258–278, which are higher than the corresponding values of 242–256 for winter HULIS. It is noted that these values are considerably smaller than those revealed by HPSEC analysis. This difference could be explained by several factors: (1) ESI–HRMS is biased towards relatively small molecules that easily deprotonated in negative ESI mode (He et al., 2023; Lin et al., 2012); and (2) SEC can provide an apparent rather than accurate molecular size of molecules due to the lack of appropriate standards for column calibration (Fan et al., 2023; Wong et al., 2017) and (3) the potential disassembly of larger molecules stabilized by weak forces during electrospray ionization of HRMS (Fan et al., 2021; Phillips et al., 2017). Nevertheless, both HRMS and HPSEC indicate that summer HULIS exhibit larger sizes than winter HULIS. Moreover, summer HULIS exhibit higher O/C_w, ranging from 0.60 to 0.66, as well as $OS_{C,w}$, ranging from −0.29 to −0.10, which exceed the respective values of 0.50 to 0.54 and −0.46 to −0.37 observed in winter HULIS. Conversely, winter HULIS display higher $AI_{mod,w}$ values (0.26–0.33) than those (0.13–0.16) for summer ones. These findings suggest that summer HULIS are characterized by a high de-

gree of oxidation, while winter HULIS exhibit stronger aromaticity.

3.3.2 Comparison of molecular composition with HMW and LMW HULIS

CHO compounds

The CHO compounds are prominent constituents within HULIS fractions, accounting for 54 % and 21 % in summer and winter HMW HULIS, respectively, whereas these proportions increase to 71 % and 38 % in LMW HULIS (Fig. 3). It is worth noting that CHO compounds that undergo deprotonation in ESI mode are likely associated with the presence of carboxyl, carbonyl, alcohol, and ester (Lin et al., 2012; Wang et al., 2018). Moreover, CHO compounds in LMW HULIS exhibit a higher oxygenation level compared to HMW HULIS, as evidenced by the higher O/C_w and $OS_{C,w}$ values. As shown in Table 2, the O/C_w for CHO in LMW HULIS are 0.55–0.64, which are higher than 0.47–0.54 observed in HMW HULIS. In contrast, the H/C_w for CHO in HMW HULIS were consistently higher than those in LMW HULIS, with values of 1.41 vs. 1.34 in summer and 1.36 vs. 1.23 in winter (Table 2). This disparity strongly suggests a higher saturation level of CHO compounds within HMW HULIS. This conclusion is further corroborated by the lower DBE_w and $AI_{mod,w}$ observed for CHO in HMW HULIS compared to LMW HULIS (Table 2). It is known

Table 2. The average values of intensity-weighted molecular weights (MWs), elemental ratios, double bond equivalents (DBEs), modified aromaticity index (AI_{mod}), and carbon oxidation state (OS_C) for tentatively identified compounds of the bulk and MW HULIS samples.

	Elemental compositions	Number of formulas	MW_w	H/C_w	O/C_w	N/C_w	S/C_w	O/N_w	O/S_w	OM/OC_w	DBE_w	DBE/C_w	$DBE\text{-}O_w$	$AI_{mod,w}$	$OS_{C,w}$
Summer **BULK**	CHO	376	276	1.39	0.59					1.91	4.69	0.39	−2.20	0.15	−0.21
	CHON	270	260	1.35	0.60	0.15		5.52		2.10	4.99	0.50	−1.17	0.27	−0.14
	CHOS	133	278	1.74	0.71		0.11		6.61	2.38	2.21	0.24	−4.41	0.02	−0.33
	CHONS	81	265	1.69	0.59	0.18	0.14	4.98	5.20	2.49	3.38	0.36	−1.95	0.09	−0.52
	Total	860	273	1.47	0.61	0.03	0.03	1.09	1.54	2.06	4.20	0.38	−2.44	0.14	−0.24
HMW	CHO	270	264	1.41	0.55					1.85	4.51	0.38	−1.70	0.16	−0.32
	CHON	264	248	1.42	0.61	0.14		5.23		2.09	4.44	0.47	−1.33	0.24	−0.20
	CHOS	72	247	1.82	0.75		0.14		5.83	2.53	1.81	0.22	−4.07	0.01	−0.32
	CHONS	39	269	1.55	0.64	0.19	0.15	4.87	5.16	2.60	3.82	0.44	−1.65	0.14	−0.28
	Total	645	258	1.48	0.60	0.05	0.03	1.70	1.07	2.05	4.09	0.39	−1.91	0.16	−0.29
LMW	CHO	365	275	1.34	0.64					1.97	4.82	0.42	−2.47	0.16	−0.05
	CHON	155	272	1.39	0.66	0.11		6.60		2.12	4.80	0.45	−2.09	0.18	−0.08
	CHOS	120	284	1.71	0.74		0.11		7.05	2.43	2.51	0.25	−4.58	0.02	−0.22
	CHONS	32	322	1.71	0.64	0.11	0.11	6.59	6.63	2.42	3.32	0.30	−3.41	0.06	−0.42
	Total	672	278	1.42	0.66	0.01	0.02	0.80	1.48	2.08	4.36	0.39	−2.84	0.13	−0.10
Winter **BULK**	CHO	142	247	1.23	0.48					1.75	5.35	0.47	−0.05	0.32	−0.26
	CHON	194	231	1.24	0.53	0.16		3.96		1.99	5.17	0.57	0.52	0.48	−0.18
	CHOS	79	271	1.93	0.51		0.11		4.97	2.14	1.21	0.14	−3.80	0.04	−0.91
	CHONS	20	271	1.61	0.69	0.16	0.13	5.60	5.90	2.60	3.32	0.40	−2.65	0.09	−0.24
	Total	435	247	1.41	0.52	0.08	0.03	2.02	1.42	1.99	4.27	0.44	−0.77	0.31	−0.37
HMW	CHO	138	232	1.36	0.47					1.74	4.79	0.41	0.02	0.28	−0.42
	CHON	244	232	1.29	0.53	0.16		3.89		2.01	4.87	0.55	0.23	0.44	−0.23
	CHOS	59	292	2.08	0.40		0.12		4.40	2.04	0.46	0.06	−4.06	0.02	−1.27
	CHONS	29	236	1.74	0.48	0.22	0.20	2.82	3.02	2.57	2.88	0.38	−0.57	0.27	−0.77
	Total	470	242	1.46	0.50	0.10	0.03	2.37	0.85	1.98	4.04	0.43	−0.57	0.33	−0.46
LMW	CHO	176	249	1.23	0.54					1.82	5.25	0.48	−0.65	0.30	−0.15
	CHON	195	239	1.34	0.49	0.16		3.99		1.95	4.88	0.52	0.29	0.45	−0.36
	CHOS	107	280	1.94	0.54		0.10		5.42	2.17	1.20	0.13	−4.25	0.02	−0.85
	CHONS	28	272	1.67	0.69	0.16	0.14	5.89	6.03	2.63	2.99	0.37	−3.15	0.13	−0.29
	Total	506	256	1.47	0.54	0.06	0.04	1.61	1.78	2.01	3.96	0.39	−1.45	0.26	−0.40

that these values serve as estimations of C=C density and aromatic and condensed aromatic structures (Zhang et al., 2021; Song et al., 2022). Taken together, the CHO compounds within HMW HULIS exhibit a more aliphatic nature but lower aromaticity and oxidation levels when compared to those within LMW HULIS.

CHON compounds

HMW HULIS fractions consist of a higher proportion of CHON compounds compared to LMW HULIS, with proportions of 27 % vs. 8 % in summer and 58 % vs. 30 % in winter (Fig. 3). This observation suggests that HMW HULIS contain a higher content of N-containing components. It is noted that the LMW HULIS are generally characterized by higher O/N_w values of 6.60 in summer and 3.99 in winter compared to 5.23 in summer and 3.89 in winter for HMW HULIS. This indicates that the CHON compounds within LMW HULIS are more highly oxidized than those within HMW HULIS. In general, compounds with $O/N \geq 3$ are indicative of oxidized N groups such as nitro ($-NO_2$) or nitrooxy ($-ONO_2$), while compounds with $O/N < 3$ may denote the reduced N-containing functional groups (i.e., amines) (He et al., 2023; Song et al., 2022; Zeng et al., 2021). In this study, a majority of the CHON compounds, comprising 73 %–85 % in summer and 59 %–64 % in winter, exhibited $O/N \geq 3$ in both MW HULIS fractions. This suggests that high concentrations of nitro compounds or organonitrates dominate the CHON compounds (Sun et al., 2023; Zeng et al., 2021; Wang et al., 2018), especially in summer samples, primarily due to the hydroxyl radical oxidation of biogenic or anthropogenic VOC precursors, as well as BB emissions (Sun et al., 2021; Song et al., 2022; Zou et al., 2023; Zhang et al., 2021). Furthermore, the CHON compounds exhibiting $O/N \geq 3$ were more abundant in LMW HULIS compared to HMW HULIS, accounting for 85 % vs. 73 % in summer and 64 % vs. 59 % in winter. In contrast, HMW HULIS contained more CHON compounds with $O/N < 3$ compared to LMW HULIS. These findings collectively indicate that the CHON within HMW HULIS possess a lower content of nitro compounds or organonitrates than LMW HULIS. Based on FTIR analysis (Text S2 and Fig. S6), it is known that HMW HULIS contain more carboxylic groups than LMW HULIS, which indicate a higher likelihood of HMW HULIS containing more amino acids.

CHOS and CHONS compounds

In this study, we observed that CHOS accounted for proportions of 13 % to 25 % in all MW HULIS fractions, while CHONS had a lower proportion of 3 % to 7 % (Fig. 3). Notably, the distribution of CHOS differed between HMW and LMW HULIS in both season samples. As depicted in Fig. 3, HMW HULIS contained fewer CHOS compounds compared to LMW HULIS, with proportions of 13 % vs. 17 % in sum-

mer and 17 % vs. 25 % in winter. This finding suggests that a greater number of CHOS compounds are incorporated into the LMW HULIS fractions, which potentially lead to a reduction in the light absorption of LMW HULIS (Zeng et al., 2021; Zhang et al., 2021). Furthermore, as indicated in Table 2, both the CHOS and CHONS within LMW HULIS exhibited higher O/S_w values than HMW HULIS in both seasonal samples. Consequently, the S-containing compounds within LMW HULIS were characterized by a higher degree of oxidation, primarily attributed to SO_2-related chemical oxidation process, in comparison to those in HMW HULIS. Moreover, it was observed that 61 % to 92 % of CHOS compounds exhibited $O/S > 4$ and 3 % to 43 % of CHONS compounds had $O/S > 7$ for all MW HULIS fractions. Among them, HMW HULIS have lower proportions of CHOS with $O/S > 4$ and CHONS with $O/S > 7$ than LMW HULIS, suggesting a reduced presence of potential organosulfates and nitrooxy organosulfates within HMW HULIS (Sun et al., 2023; Zeng et al., 2021; Zou et al., 2023; Wang et al., 2018).

3.3.3   Comparative analysis of unique molecular formulas in HMW and LMW HULIS

In this study, particular emphasis was placed on the unique molecular formulas within the HMW or LMW HULIS fractions. Figure 4a and b illustrate the van Krevelen (VK) diagram depicting the distribution of unique molecular formulas within HMW and LMW HULIS in summer and winter samples. It is evident that a majority of unique formulas within LMW HULIS are concentrated around the origin with $O/C > 0.5$, accounting for 83 % in summer and 64 % in winter. In contrast, most formulas within HMW HULIS exhibited $O/C < 0.5$, representing about 58 % for both seasonal samples. These findings indicate that the unique molecules within LMW HULIS consist of more polar O-containing organic compounds than those within HMW HULIS.

The molecular formulas are further categorized into seven groups based on previous studies, including lignin-like species, protein/amino sugars, condensed aromatics, tannin-like species, carbohydrate-like species, unsaturated hydrocarbons, and lipid-like species (He et al., 2023; Sun et al., 2023, 2021). The classification rules for these formulas can be found in Table S2. Figure 4c provides an overview of the relative contributions of the number of unique formulas from each of the seven groups for HMW and LMW HULIS. The results indicate that the dominant substance class in the unique formulas within both MW HULIS are lignin-like species, accounting for proportions of 31 %–40 %. This finding indicates that lignin derivatives are fundamental components in both HMW and LMW HULIS either in summer or winter aerosols. Additionally, there are notable differences in the molecular characteristics of lignin-like species within HMW and LMW HULIS. As listed in Table S3, lignin-like species within HMW HULIS exhibit lower MW_w and O/C_w but higher N/C_w and $AI_{mod,w}$ values than those within LMW
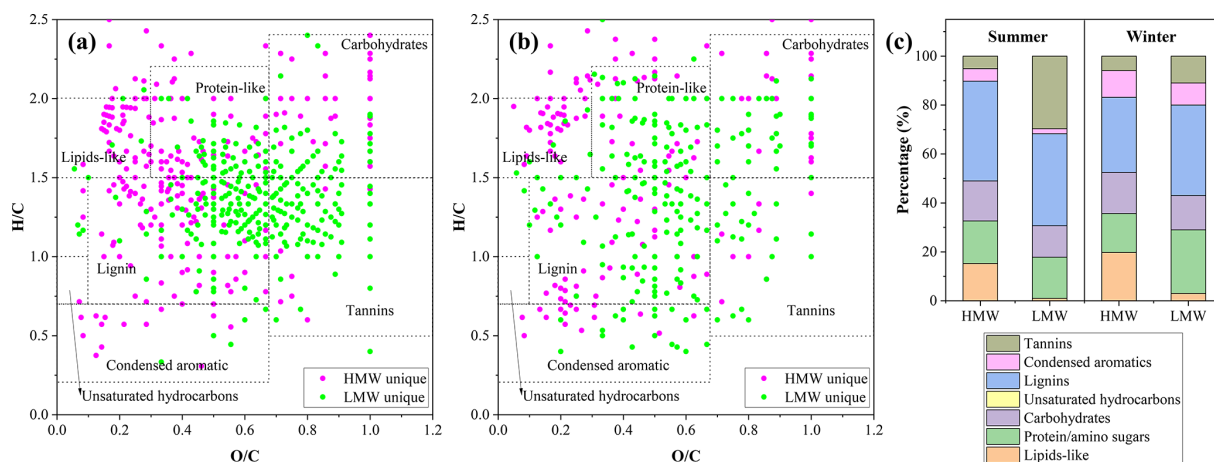
Figure 4. Van Krevelen diagrams for the unique molecular formulas within HMW and LMW HULIS from **(a)** summer and **(b)** winter aerosols. **(c)** The contributions of major substances classes in unique formulas.

HULIS in both seasonal samples. These observations suggest that the unique lignin-like substances in HMW HULIS likely contain more N-enriched and highly aromatic species, while those in LMW HULIS tend to concentrate more aliphatic O-containing compounds. These distinctions in composition and characteristics between HMW and LMW HULIS fractions provide valuable insights into their origins and transformations in the atmosphere.

Moreover, there are notable variations in the contributions of lipid-like, protein/amino sugars, carbohydrates, condensed aromatics, and tannin species between HMW and LMW HULIS. In general, HMW HULIS have a higher proportion of lipid-like species, carbohydrates, and condensed aromatics than LMW HULIS in both summer and winter aerosols. Among these, the most remarkable difference in composition between HMW HULIS and LMW HULIS is seen in lipid-like species, accounting for 15 % versus 1 % in summer and 20 % versus 3 % in winter (Fig. 4). As reported in previous studies, lipid-like species primarily originate from biogenic emissions (Sun et al., 2021; He et al., 2023; Li et al., 2022). This suggests that there is a stronger contribution from biogenic emissions to HMW HULIS. Additionally, these species in HMW HULIS were usually characterized by lower DBE_w and slightly lower $OS_{C,w}$ when compared to LMW HULIS (Table S3), indicating they present stronger saturation and fewer oxidized substituents. On the other hand, tannin species contribute a higher proportion to LMW HULIS, constituting 30 % in summer and 11 % in winter, while comprising only 5 %–6 % in HMW HULIS in both season aerosols. Tannin-like species are known to consist of various polyphenolic groups containing hydroxyl and carboxylic functional groups (Sun et al., 2021; He et al., 2023; Li et al., 2022; Ning et al., 2019). The slightly lower DBE_w but much higher $DBE–O_w$ values for unique tannin-like species within HMW HULIS were observed compared to LMW HULIS (Table S3), suggesting that the former ones

are enriched in more unsaturated O-containing functional groups, particularly the carboxylic functional groups.

3.4 Atmospheric implications

This study provides comprehensive comparison between HMW and LMW HULIS regarding their distributions, chemical structures, molecular sizes, and compositions. HMW HULIS appear to be larger than LMW HULIS, as evidenced by both ultrafiltration natures and the MW distributions of chromophores analyzed by HPSEC. However, HRMS analysis revealed that the average MW_w of identified formulas within HMW HULIS were lower than those of LMW HULIS (Table 2). This discrepancy can likely be attributed to the "assembled structures" that construct the aerosol HULIS, as suggested in many previous studies focusing on HULIS and BrC characterization (Phillips et al., 2017; Fan et al., 2021, 2023; Qin et al., 2022). In fact, the results from EEM–FRI and FTIR analysis support the notion that HMW and LMW HULIS likely consist of potential structures assembled by similar basic fluorophores and functional groups. Based on this theory, HMW HULIS may consist of macromolecular species primarily assembled from small molecules through weak forces (i.e., π–π, van der Waals, hydrophobic, or hydrogen bonds) and/or charge–transfer interactions (Fan et al., 2021; Phillips et al., 2017), which can potentially disassemble during ESI ionization and form low MW molecules.

Based on the molecular-level characterization, significant distinctions in properties between HMW HULIS and LMW HULIS become evident. HMW HULIS generally exhibit stronger aromaticity but a lower oxidation degree when compared to LMW HULIS. In terms of molecular composition, HMW HULIS contain higher quantities of CHON species but lower quantities of CHO compounds than LMW HULIS. Furthermore, more lipid-like species were identified as unique molecules in HMW HULIS, while more tannin-

like species with abundant carboxylic groups were observed as unique molecules in LMW HULIS. Given these pronounced differences between HMW and LMW HULIS, it can be speculated that the higher levels of aromatic structures, greater presence of CHON molecules and the presence of lipid-like species may serve as driving factors in the formation of potential assembled structures in HMW HULIS. Additionally, it is well established that CHON can enhance the light absorption of organic aerosols (OAs), while CHO species may have the opposite effect, weakening light absorption (Song et al., 2022; He et al., 2023; Wang et al., 2019; Zeng et al., 2021). Therefore, it is reasonable to conclude that HMW HULIS possess stronger light absorbing capability, which is consistent with their larger MAE_{365} values.

Importantly, HMW HULIS contain higher numbers of carboxylic functional groups, reduced nitrogen species (e.g., amines), and aromatic species than LMW HULIS. These functional groups have strong complexation abilities with transition metals (Wang et al., 2021a, b), thus influencing the transformation and chemical behavior of metals. Moreover, the OA metal complex can potentially enhance the catalytic generation of reactive oxygen species (ROS) in organic aerosols (Win et al., 2018; Zhang et al., 2022a), thereby playing significant roles in adverse health effects of OA. These results reinforce the significance of HMW HULIS in light absorption, metal complexation, and the potential ROS-generation ability of aerosol BrC.

4   Conclusions

This study successfully isolated and characterized HMW and LMW HULIS in atmospheric aerosols using the UF–SPE technique, yielding insights into their distribution, optical properties, and molecular-level characteristics. Both HMW and LMW HULIS exhibited a continuum of MW distributions, ranging from 100 to 20 000 Da. However, HMW HULIS displayed more extensive and intricate MW distributions, suggesting differences in their sources and formation processes compared to LMW HULIS. In general, HMW HULIS constituted a higher percentage of TOC and UV254 in aerosols compared to LMW HULIS, indicating the prevalence of hydrophobic and conjugated aromatic structures in the former. Moreover, HMW HULIS exhibited higher aromaticity, stronger light absorption abilities, weaker spectra dependence, and stronger humification and conjugation compared to LMW HULIS. Interestingly, HRMS analysis revealed slightly lower MW_w values for HMW HULIS than LMW HULIS, which contradicted the HPSEC results and the nature of UF fractionation. This finding strongly suggests the possibility of small molecules assembling to form macromolecules in HMW HULIS. Regarding molecular composition, HMW HULIS contained a higher proportion of CHON compounds, constituting 27 % vs. 8 % in summer and 58 % vs. 30 % in winter, while LMW HULIS were primarily composed of CHO compounds, accounting for 71 % vs. 54 % in summer and 38 % vs. 21 % in winter. Both HMW and LMW HULIS featured lignin-like substances as major unique molecular formulas, but HMW HULIS exhibited more N-enriched and highly aromatic species, whereas LMW HULIS contained a higher proportion of polar O-containing functional groups. Additionally, HMW HULIS included a greater number of unique lipid-like compounds, while LMW HULIS tend to concentrate more tannin-like compounds. These observations shed light on the complex nature of MW HULIS and their diverse sources and transformations. Future research should expand the geographical and seasonal coverage to gain a more comprehensive understanding of the molecular-level characteristics of MW HULIS in various atmospheric environments. Furthermore, exploring additional physicochemical properties of MW HULIS will provide valuable insights into their potential health and environmental implications. Overall, this study offers valuable insights into the molecular-level characteristics of aerosol HULIS, enhancing our understanding of their evolution, sources, and potential environmental effects.

Author contributions. XF: methodology, supervision, funding acquisition, review and editing. AC: sampling and data curation. XY: review and editing. TC: sampling and investigation. DC: investigation and data curation. WJ: formal analysis. YC: review and editing. FM: review and editing. JS: methodology, review, and editing. PP: review and editing.

References

Bao, M., Zhang, Y.-L., Cao, F., Lin, Y.-C., Hong, Y., Fan, M., Zhang, Y., Yang, X., and Xie, F.: Light absorption and source apportionment of water soluble humic-like substances (HULIS) in $PM_{2.5}$ at Nanjing, China, Environ. Res., 206, 112554, https://doi.org/10.1016/j.envres.2021.112554, 2022.

Birdwell, J. E. and Valsaraj, K. T.: Characterization of dissolved organic matter in fogwater by excitation–emission matrix fluorescence spectroscopy, Atmos. Environ., 44, 3246–3253, 2010.

Cao, T., Li, M., Zou, C., Fan, X., Song, J., Jia, W., Yu, C., Yu, Z., and Peng, P.: Chemical composition, optical properties, and oxidative potential of water- and methanol-soluble organic compounds emitted from the combustion of biomass materials and coal, Atmos. Chem. Phys., 21, 13187–13205, https://doi.org/10.5194/acp-21-13187-2021, 2021.

Cao, T., Li, M., Xu, C., Song, J., Fan, X., Li, J., Jia, W., and Peng, P.: Technical note: Chemical composition and source identification of fluorescent components in atmospheric water-soluble brown carbon by excitation–emission matrix spectroscopy with parallel factor analysis – potential limitations and applications, Atmos. Chem. Phys., 23, 2613–2625, https://doi.org/10.5194/acp-23-2613-2023, 2023.

Chen, J., Wu, Z. J., Zhao, X., Wang, Y. J., Chen, J. C., Qiu, Y. T., Zong, T. M., Chen, H. X., Wang, B. B., Lin, P., Liu, W., Guo, S., Yao, M. S., Zeng, L. M., Wex, H., Liu, X., Hu, M., and Li, S. M.: Atmospheric Humic-Like Substances (HULIS) Act as Ice Active Entities, Geophys. Res. Lett., 48, e2021GL092443, https://doi.org/10.1029/2021GL092443, 2021a.

Chen, Q., Hua, X., and Dyussenova, A.: Evolution of the chromophore aerosols and its driving factors in summertime Xi'an, Northwest China, Chemosphere, 281, 130838, https://doi.org/10.1016/j.chemosphere.2021.130838, 2021b.

Chen, W., Westerhoff, P., Leenheer, J. A., and Booksh, K.: Fluorescence Excitation-Emission Matrix Regional Integration to Quantify Spectra for Dissolved Organic Matter, Environ. Sci. Technol., 37, 5701–5710, 2003.

Di Lorenzo, R. A., Washenfelder, R. A., Attwood, A. R., Guo, H., Xu, L., Ng, N. L., Weber, R. J., Baumann, K., Edgerton, E., and Young, C. J.: Molecular-Size-Separated Brown Carbon Absorption for Biomass-Burning Aerosol at Multiple Field Sites, Environ. Sci. Technol., 51, 3128–3137, 2017.

Di Lorenzo, R. A., Place, B. K., VandenBoer, T. C., and Young, C. J.: Composition of Size-Resolved Aged Boreal Fire Aerosols: Brown Carbon, Biomass Burning Tracers, and Reduced Nitrogen, ACS Earth Space Chem., 2, 278–285, 2018.

Dinar, E., Taraniuk, I., Graber, E. R., Anttila, T., Mentel, T. F., and Rudich, Y.: Hygroscopic growth of atmospheric and model humic-like substances, J. Geophys. Res.-Atmos., 112, D05211, https://doi.org/10.1029/2006JD007442, 2007.

Fan, X., Song, J., and Peng, P.: Comparative study for separation of atmospheric humic-like substance (HULIS) by ENVI-18, HLB, XAD-8 and DEAE sorbents: elemental composition, FT-IR, 1H NMR and off-line thermochemolysis with tetramethylammonium hydroxide (TMAH), Chemosphere, 93, 1710–1719, 2013.

Fan, X., Song, J., and Peng, P. a.: Temporal variations of the abundance and optical properties of water soluble Humic-Like Substances (HULIS) in $PM_{2.5}$ at Guangzhou, China, Atmos. Res., 172–173, 8–15, 2016a.

Fan, X., Wei, S., Zhu, M., Song, J., and Peng, P.: Comprehensive characterization of humic-like substances in smoke $PM_{2.5}$ emitted from the combustion of biomass materials and fossil fuels, Atmos. Chem. Phys., 16, 13321–13340, https://doi.org/10.5194/acp-16-13321-2016, 2016b.

Fan, X., Li, M., Cao, T., Cheng, C., Li, F., Xie, Y., Wei, S., Song, J., and Peng, P. a.: Optical properties and oxidative potential of water- and alkaline-soluble brown carbon in smoke particles emitted from laboratory simulated biomass burning, Atmos. Environ., 194, 48–57, 2018.

Fan, X., Yu, X., Wang, Y., Xiao, X., Li, F., Xie, Y., Wei, S., Song, J., and Peng, P. a.: The aging behaviors of chromophoric biomass burning brown carbon during dark aqueous hydroxyl radical oxidation processes in laboratory studies, Atmos. Environ., 205, 9–18, 2019.

Fan, X., Cao, T., Yu, X., Wang, Y., Xiao, X., Li, F., Xie, Y., Ji, W., Song, J., and Peng, P.: The evolutionary behavior of chromophoric brown carbon during ozone aging of fine particles from biomass burning, Atmos. Chem. Phys., 20, 4593–4605, https://doi.org/10.5194/acp-20-4593-2020, 2020.

Fan, X., Cai, F., Xu, C., Yu, X., Wang, Y., Xiao, X., Ji, W., Cao, T., Song, J., and Peng, P. a.: Molecular weight-dependent abundance, absorption, and fluorescence characteristics of water-soluble organic matter in atmospheric aerosols, Atmos. Environ., 247, 118159, https://doi.org/10.1016/j.atmosenv.2020.118159, 2021.

Fan, X., Cheng, A., Chen, D., Cao, T., Ji, W., Song, J., and Peng, P.: Investigating the molecular weight distribution of atmospheric water-soluble brown carbon using high-performance size exclusion chromatography coupled with diode array and fluorescence detectors, Chemosphere, 338, 139517, https://doi.org/10.1016/j.chemosphere.2023.139517, 2023.

Fan, X. J., Song, J. Z., and Peng, P. a.: Comparison of isolation and quantification methods to measure humic-like substances (HULIS) in atmospheric particles, Atmos. Environ., 60, 366–374, 2012.

Graber, E. R. and Rudich, Y.: Atmospheric HULIS: How humic-like are they? A comprehensive and critical review, Atmos. Chem. Phys., 6, 729–753, https://doi.org/10.5194/acp-6-729-2006, 2006.

He, T., Wu, Y., Wang, D., Cai, J., Song, J., Yu, Z., Zeng, X., and Peng, P. a.: Molecular compositions and optical properties of water-soluble brown carbon during the autumn and winter in Guangzhou, China, Atmos. Environ., 296, 119573, https://doi.org/10.1016/j.atmosenv.2022.119573, 2023.

Huo, Y., Wang, Y., Qi, W., Jiang, M., and Li, M.: Comprehensive characterizations of HULIS in fresh and secondary emissions of crop straw burning, Atmos. Environ., 248, 118220, https://doi.org/10.1016/j.atmosenv.2021.118220, 2021.

Kawasaki, N., Matsushige, K., Komatsu, K., Kohzu, A., Nara, F. W., Ogishi, F., Yahata, M., Mikami, H., Goto, T., and Imai, A.: Fast and precise method for HPLC–size exclusion chromatography with UV and TOC (NDIR) detection: Importance of multiple detectors to evaluate the characteristics of dissolved organic matter, Water Res., 45, 6240–6248, 2011.

Kumar, V., Goel, A., and Rajput, P.: Compositional and surface characterization of HULIS by UV-Vis, FTIR, NMR and XPS: Wintertime study in Northern India, Atmos. Environ., 164, 468–475, 2017.

Li, X., Yu, F., Cao, J., Fu, P., Hua, X., Chen, Q., Li, J., Guan, D., Tripathee, L., Chen, Q., and Wang, Y.: Chromophoric dissolved organic carbon cycle and its molecular compositions and optical properties in precipitation in the Guanzhong basin, China, Sci. Total Environ., 814, 152775, https://doi.org/10.1016/j.scitotenv.2021.152775, 2022.

Lin, P., Rincon, A. G., Kalberer, M., and Yu, J. Z.: Elemental composition of HULIS in the Pearl River Delta Region, China: results inferred from positive and negative electrospray high resolution mass spectrometric data, Environ. Sci. Technol., 46, 7454–7462, 2012.

Ma, Y., Cheng, Y., Qiu, X., Cao, G., Kuang, B., Yu, J. Z., and Hu, D.: Optical properties, source apportionment and redox activity of humic-like substances (HULIS) in airborne fine particulates in Hong Kong, Environ. Pollut., 255, 113087, https://doi.org/10.1016/j.envpol.2019.113087, 2019.

Mukherjee, A., Dey, S., Rana, A., Jia, S., Banerjee, S., and Sarkar, S.: Sources and atmospheric processing of brown carbon and HULIS in the Indo-Gangetic Plain: Insights from compositional analysis, Environ. Pollut., 267, 115440, https://doi.org/10.1016/j.envpol.2020.115440, 2020.

Ning, C., Gao, Y., Zhang, H., Yu, H., Wang, L., Geng, N., Cao, R., and Chen, J.: Molecular characterization of dissolved organic matters in winter atmospheric fine particulate matters (PM$_{2.5}$) from a coastal city of northeast China, Sci. Total Environ., 689, 312–321, 2019.

Phillips, S. M., Bellcross, A. D., and Smith, G. D.: Light Absorption by Brown Carbon in the Southeastern United States is pH-dependent, Environ. Sci. Technol., 51, 6782–6790, 2017.

Piccolo, A.: The supramolecular structure of humic substances: A novel understanding of humus chemistry and implications in soil science, Adv. Agron., 75, 57–134, https://doi.org/10.1016/S0065-2113(02)75003-7, 2002.

Qin, J., Zhang, L., Zhou, X., Duan, J., Mu, S., Xiao, K., Hu, J., and Tan, J.: Fluorescence fingerprinting properties for exploring water-soluble organic compounds in PM$_{2.5}$ in an industrial city of northwest China, Atmos. Environ., 184, 203–211, 2018.

Qin, J., Zhang, L., Qin, Y., Shi, S., Li, J., Gao, Y., Tan, J., and Wang, X.: pH-Dependent Chemical Transformations of Humic-Like Substances and Further Cognitions Revealed by Optical Methods, Environ. Sci. Technol., 56, 7578–7587, 2022.

Santos, P. S. M., Otero, M., Duarte, R. M. B. O., and Duarte, A. C.: Spectroscopic characterization of dissolved organic matter isolated from rainwater, Chemosphere, 74, 1053–1061, 2009.

Santos, P. S. M., Santos, E. B. H., and Duarte, A. C.: First spectroscopic study on the structural features of dissolved organic matter isolated from rainwater in different seasons, Sci. Total Environ., 426, 172–179, 2012.

Song, J., Li, M., Jiang, B., Wei, S., Fan, X., and Peng, P.: Molecular Characterization of Water-Soluble Humic like Substances in Smoke Particles Emitted from Combustion of Biomass Materials and Coal Using Ultrahigh-Resolution Electrospray Ionization Fourier Transform Ion Cyclotron Resonance Mass Spectrometry, Environ. Sci. Technol., 52, 2575–2585, 2018.

Song, J., Li, M., Zou, C., Cao, T., Fan, X., Jiang, B., Yu, Z., Jia, W., and Peng, P. a.: Molecular Characterization of Nitrogen-Containing Compounds in Humic-like Substances Emitted from Biomass Burning and Coal Combustion, Environ. Sci. Technol., 56, 119–130, 2022.

Song, J. Z., Huang, W. L., Peng, P. a., Xiao, B. H., and Ma, Y. J.: Humic Acid Molecular Weight Estimation by High-Performance Size-Exclusion Chromatography with Ultraviolet Absorbance Detection and Refractive Index Detection, Soil Sci. Soc. Am. J., 74, 2013–2020, 2010.

Sun, H., Li, X., Zhu, C., Huo, Y., Zhu, Z., Wei, Y., Yao, L., Xiao, H., and Chen, J.: Molecular composition and optical property of humic-like substances (HULIS) in winter-time PM$_{2.5}$ in the rural area of North China Plain, Atmos. Environ., 252, 118316, https://doi.org/10.1016/j.atmosenv.2021.118316, 2021.

Sun, H., Wu, Z., Kang, X., Zhu, C., Yu, L., Li, R., Lin, Z., and Chen, J.: Molecular characterization of humic-like substances (HULIS) in atmospheric particles (PM$_{2.5}$) in offshore Eastern China Sea (OECS) using solid-phase extraction coupled with ESI FT-ICR MS, Atmos. Environ., 294, 119523, https://doi.org/10.1016/j.atmosenv.2022.119523, 2023.

Wang, K., Zhang, Y., Huang, R.-J., Cao, J., and Hoffmann, T.: UHPLC-Orbitrap mass spectrometric characterization of organic aerosol from a central European city (Mainz, Germany) and a Chinese megacity (Beijing), Atmos. Environ., 189, 22–29, 2018.

Wang, X., Qin, Y., Qin, J., Long, X., Qi, T., Chen, R., Xiao, K., and Tan, J.: Spectroscopic insight into the pH-dependent interactions between atmospheric heavy metals (Cu and Zn) and water-soluble organic compounds in PM$_{2.5}$, Sci. Total Environ., 767, 145261, https://doi.org/10.1016/j.scitotenv.2021.145261, 2021a.

Wang, X., Qin, Y. Y., Qin, J. J., Yang, Y. R., Qi, T., Chen, R. Z., Tan, J. H., and Xiao, K.: The interaction laws of atmospheric heavy metal ions and water-soluble organic compounds in PM$_{2.5}$ based on the excitation-emission matrix fluorescence spectroscopy, J. Hazard. Mater., 402, 123497, https://doi.org/10.1016/j.jhazmat.2020.123497, 2021b.

Wang, Y., Hu, M., Lin, P., Tan, T., Li, M., Xu, N., Zheng, J., Du, Z., Qin, Y., Wu, Y., Lu, S., Song, Y., Wu, Z., Guo, S., Zeng, L., Huang, X., and He, L.: Enhancement in Particulate Organic Nitrogen and Light Absorption of Humic-Like Substances over Tibetan Plateau Due to Long-Range Transported Biomass Burning Emissions, Environ. Sci. Technol., 53, 14222–14232, 2019.

Win, M. S., Tian, Z., Zhao, H., Xiao, K., Peng, J., Shang, Y., Wu, M., Xiu, G., Lu, S., Yonemochi, S., and Wang, Q.: Atmospheric HULIS and its ability to mediate the reactive oxygen species (ROS): A review, J. Environ. Sci.-China, 71, 13–31, 2018.

Wong, J. P. S., Nenes, A., and Weber, R. J.: Changes in Light Absorptivity of Molecular Weight Separated Brown Carbon Due to Photolytic Aging, Environ. Sci. Technol., 51, 8414–8421, 2017.

Wong, J. P. S., Tsagkaraki, M., Tsiodra, I., Mihalopoulos, N., Violaki, K., Kanakidou, M., Sciare, J., Nenes, A., and Weber, R. J.: Atmospheric evolution of molecular-weight-separated brown carbon from biomass burning, Atmos. Chem. Phys., 19, 7319–7334, https://doi.org/10.5194/acp-19-7319-2019, 2019.

Wu, G., Wan, X., Gao, S., Fu, P., Yin, Y., Li, G., Zhang, G., Kang, S., Ram, K., and Cong, Z.: Humic-Like Substances (HULIS) in Aerosols of Central Tibetan Plateau (Nam Co, 4730 m asl): Abundance, Light Absorption Properties, and Sources, Environ. Sci. Technol., 52, 7203–7211, 2018.

Wu, G., Wan, X., Ram, K., Li, P., Liu, B., Yin, Y., Fu, P., Loewen, M., Gao, S., Kang, S., Kawamura, K., Wang, Y., and Cong, Z.: Light absorption, fluorescence properties and sources of brown carbon aerosols in the Southeast Tibetan Plateau, Environ. Pollut., 257, 113616, https://doi.org/10.1016/j.envpol.2019.113616, 2020.

Wu, G., Fu, P., Ram, K., Song, J., Chen, Q., Kawamura, K., Wan, X., Kang, S., Wang, X., Laskin, A., and Cong, Z.: Fluorescence characteristics of water-soluble organic carbon in atmospheric aerosol?, Environ. Pollut., 268, 115906, https://doi.org/10.1016/j.envpol.2020.115906, 2021.

Yuan, W., Huang, R.-J., Yang, L., Ni, H., Wang, T., Cao, W., Duan, J., Guo, J., Huang, H., and Hoffmann, T.: Concentrations, optical properties and sources of humic-like substances (HULIS) in fine particulate matter in Xi'an, Northwest China, Sci. Total Environ., 789, 147902, https://doi.org/10.1016/j.scitotenv.2021.147902, 2021.

Zeng, Y., Ning, Y., Shen, Z., Zhang, L., Zhang, T., Lei, Y., Zhang, Q., Li, G., Xu, H., Ho, S. S. H., and Cao, J.: The Roles of N, S, and O in Molecular Absorption Features of Brown Carbon in PM$_{2.5}$ in a Typical Semi-Arid Megacity in Northwestern China, J. Geophys. Res.-Atmos., 126, e2021JD034791, https://doi.org/10.1029/2021JD034791, 2021.

Zhang, T., Shen, Z., Zhang, L., Tang, Z., Zhang, Q., Chen, Q., Lei, Y., Zeng, Y., Xu, H., and Cao, J.: PM$_{2.5}$ Humic-like substances over Xi'an, China: Optical properties, chemical functional group, and source identification, Atmos. Res., 234, 104784, https://doi.org/10.1016/j.atmosres.2019.104784, 2020.

Zhang, T., Shen, Z., Zeng, Y., Cheng, C., Wang, D., Zhang, Q., Lei, Y., Zhang, Y., Sun, J., Xu, H., Ho, S. S. H., and Cao, J.: Light absorption properties and molecular profiles of HULIS in PM$_{2.5}$ emitted from biomass burning in traditional "Heated Kang" in Northwest China, Sci. Total Environ., 776, 146014, https://doi.org/10.1016/j.scitotenv.2021.146014, 2021.

Zhang, T., Huang, S., Wang, D., Sun, J., Zhang, Q., Xu, H., Hang Ho, S. S., Cao, J., and Shen, Z.: Seasonal and diurnal variation of PM$_{2.5}$ HULIS over Xi'an in Northwest China: Optical properties, chemical functional group, and relationship with reactive oxygen species (ROS), Atmos. Environ., 268, 118782, https://doi.org/10.1016/j.atmosenv.2021.118782, 2022a.

Zhang, T., Shen, Z., Huang, S., Lei, Y., Zeng, Y., Sun, J., Zhang, Q., Ho, S. S. H., Xu, H., and Cao, J.: Optical properties, molecular characterizations, and oxidative potentials of different polarity levels of water-soluble organic matters in winter PM$_{2.5}$ in six China's megacities, Sci. Total Environ., 853, 158600, https://doi.org/10.1016/j.scitotenv.2022.158600, 2022b.

Zhang, W., Li, L., Wang, D., Wang, R., Yu, S., and Gao, N.: Characterizing dissolved organic matter in aquatic environments by size exclusion chromatography coupled with multiple detectors, Anal. Chim. Acta, 1191, 339358, https://doi.org/10.1016/j.aca.2021.339358, 2022.

Zheng, G. J., He, K. B., Duan, F. K., Cheng, Y., and Ma, Y. L.: Measurement of humic-like substances in aerosols: A review, Environ. Pollut., 181, 301–314, 2013.

Zou, C., Li, M., Cao, T., Zhu, M., Fan, X., Peng, S., Song, J., Jiang, B., Jia, W., Yu, C., Song, H., Yu, Z., Li, J., Zhang, G., and Peng, P. a.: Comparison of solid phase extraction methods for the measurement of humic-like substances (HULIS) in atmospheric particles, Atmos. Environ., 225, 117370, https://doi.org/10.1016/j.atmosenv.2020.117370, 2020.

Zou, C., Cao, T., Li, M., Song, J., Jiang, B., Jia, W., Li, J., Ding, X., Yu, Z., Zhang, G., and Peng, P.: Measurement report: Changes in light absorption and molecular composition of water-soluble humic-like substances during a winter haze bloom-decay process in Guangzhou, China, Atmos. Chem. Phys., 23, 963–979, https://doi.org/10.5194/acp-23-963-2023, 2023.